LOW TEMPERATURE THERMOLUMINESCENCE PROPERTIES OF Al-DOPED ZnO NANOPARTICLES

A MASTER'S THESIS

in

Chemical Engineering and Applied Chemistry Department

Atılım University

by

NAHED EMHEMED

APRIL 2018

LOW TEMPERATURE THERMOLUMINESCENCE PROPERTIES OF Al-DOPED ZnO NANOPARTICLES

A THESIS SUBMITTED TO

THE GRADUATE SCHOOL OF NATURAL AND APPLIED SCIENCES

OF

ATILIM UNIVERSITY

BY

NAHED EMHEMED

IN PARTIAL FULFILLMENT OF THE REQUIREMENTS FOR THE DEGREE OF

MASTER OF SCIENCE

IN

APPLIED CHEMISTRY

AT

CHEMICAL ENGINEERING AND APPLIED CHEMISTRY DEPARTMENT

APRIL 2018

Approval of the Graduate School of Natural and Applied Sciences, Atılım University.

_____

Prof. Dr. Ali Kara

Director

I certify that this thesis satisfies all the requirements as a thesis for the degree of Master of Science.

_____

Prof. Dr. Atilla Cihaner

Head of Department

This is to certify that we have read the thesis "LOW TEMPERATURE THERMOLUMINESCENCE PROPERTIES OF Al-DOPED ZnO NANOPARTICLES" submitted by "NAHED EMHEMED" and that in our opinion it is fully adequate, in scope and quality, as a thesis for the degree of Master of Science.

_____

Assoc. Prof. Dr. Mehmet Işık

Supervisor

Examining Committee Members

Prof. Dr. Nizami Hasanli _____

Prof. Dr. Atilla Cihaner _____

Assoc. Prof. Dr. Belgin İşgör _____

Assoc. Prof. Dr. Seha Tirkeş _____

Assoc. Prof. Dr. Mehmet Işık _____

Date: 19.04.2018

I declare and guarantee that all data, knowledge and information in this document has been obtained, processed and presented in accordance with academic rules and ethical conduct. Based on these rules and conduct, I have fully cited and referenced all material and results that are not original to this work.

Name, Last name: NAHED EMHEMED

Signature:

ABSTRACT

LOW TEMPERATURE THERMOLUMINESCENCE PROPERTIES OF Al-DOPED ZnO NANOPARTICLES

Emhemed, Nahed

M.Sc., Department of Chemical Engineering and Applied Chemistry

Supervisor: Assoc. Prof. Dr. Mehmet Işık

April 2018, 42 pages

ZnO nanoparticles doped with aluminium (AZO nanoparticles) were investigated using low temperature thermoluminescence (TL) and structural characterization experiments. Structural properties were studied using x-ray diffraction and scanning electron microscopy experiments. The crystal structure of the AZO nanoparticles was found as hexagonal. XRD diffraction pattern did not present any peak related with doped element. This indicated that doping was successfully carried out. Scanning electron microscopy measurements presented the surface morphology of the nanoparticles and dimensions of nanoparticles were recorded around 100 nm.

Low temperature TL experiments were performed on AZO nanoparticles in the temperature range of 10-300 K. TL curve presented one intensive peak around 123 K and two overlapped peaks to intensive peak around 85 K and 150 K. Curve fitting, initial rise, peak shape and different heating rate methods were used to find the activation energies of associated trapping centers. Analyses resulted in the presence of three centers at 44, 76 and 165 meV with peak maximum temperatures of 86.2, 121.5 and 147.1 K, respectively. Peak shape method analyses indicated that μ_g parameter for observed peaks were between 0.42 and 0.52 indicating the presence of general order of kinetics. TL experiments were also

expanded using different heating rates between 0.1 K/s and 0.7 K/s. Activation energies of trapping centers were obtained using heating rate dependency of peak maximum temperature.

Keywords: ZnO nanoparticles, Thermoluminescence, Defects

ÖZ

Al-KATKILI ZnO NANOPARÇACIKLARIN DÜŞÜK SICAKLIK TERMOLÜMİNESANS ÖZELLİKLERİ

Emhemed, Nahed

Yüksek Lisans, Kimya Mühendisliği ve Uygulamalı Kimya Bölümü

Tez Yöneticisi: Doç. Dr. Mehmet Işık

Nisan 2018, 42 sayfa

Alüminyum katkılı ZnO nanoparçacıklar (AZO nanoparçacıklar) düşük sıcaklık termolüminesans (TL) ve yapısal karakterizayon deneyleri kullanılarak incelendi. Yapısal özellikleri x-ışını kırınımı ve tarayıcı elektron mikroskobu deneyleri kullanılarak çalışıldı. AZO nanoparçacıkların kristal yapısı hegzagonal yapı olarak bulundu. X-ışını deseni katkılanan elemente ait herhangi bir pik göstermedi. Bu katkılamanın başarılı bir şekilde gerçekleştiğini gösterdi. Tarayıcı elektron mikroskobu ölçümleri nanoparçacıkların yüzek morfolojisini gösterdi ve nanoparçaıkların boyutlarının 100 nm civarında olduğu görüldü.

Düşük sıcaklık TL deneyleri AZO nanoparçacıkları üzerinde 10-300 K sıcaklık aralığında gerçekleştirildi. TL eğrisi 123 K civarında şiddetli bir pik ve bu pike çakışık 85 K ve 150 K civarında iki pik gösterdi. Eğri fit, ilk yükselme, pik şekli ve farklı ısıtma oranı metotları ilgili tuzak merkezlerinin aktivasyon enerjilerini bulmak için kullanıldı. Analizler pik maksimum sıcaklıları 86.2, 121.5 ve 147.1 K olan 44, 76 ve 165 meV seviyelerinde üç merkezin varlığını gösterdi. Pik şekli metodu analizleri, gözlemlenen pikler için μ_g parametresinin genel kinetik merterbesini işaret eden 0.42 ve 0.52 arasında olduğunu gösterdi. TL deneyleri 0.1 K/s ve 0.7 K/s arasında farklı ısıtma oranları kullanılarak genişletildi. Tuzak

merkezlerinin aktivasyon enerjileri pik maksimum sıcaklığının ısıtma hızına bağımlılığı kullanılarak eld edildi.

Anahtar Kelimeler: ZnO nanoparçacıklar, Termolüminesans, Kusurlar

TABLE OF CONTENTS

LIST OF TABLES

TABLE

LIST OF FIGURES

FIGURES

CHAPTER I

INTRODUCTION

ZnO is a semiconducting material which has a band gap of 3.37 eV at room temperature and high exciton binding energy of 60 meV. The studies on the technological application of ZnO which can be grown in different structures as crystal, thin film, nanoparticle, nanorod and nanotube have shown a great increase. Solar cells, sensors, light emitting diodes, lasers, biomedical applications are some of the important technological areas in which ZnO material is used due to its optical, electrical and piezoelectrical properties. It is clear that ZnO would carry on its importance in the next years when the advantages of properties of ZnO material as growing in different forms, wide application areas, low cost and not having toxic effect were taken into account.

ZnO is an effective material due to its enthusiastic optical and electrical properties. Its popularity in the technological applications takes the attention of scientists. In the literature, there are thousands of papers on ZnO material. Fundamental properties of ZnO giving this material advantages in the technological applications are given below.

- Direct and wide band gap

  The band gap energy of ZnO at room temperature is reported as 3.37 eV and at low temperatures as 3.44 eV [1]. Thanks to its band gap energy value, ZnO has been an effective material used in light emitting diodes, laser diodes and optoelectronic devices [2].

- Big exciton binding energy

  The exciton binding energy of ZnO semiconducting material is found as 60 meV [1]. This big binding energy shows that an effective excitonic emission takes place in ZnO at and above room temperature. This big

energy makes ZnO a promising material for optical devices based on excitonic effects [3].

- Big piezoelectric constant

  In the piezoelectric materials, a strain applied on the material creates potential difference across the material or a potential difference applied on material creates a deformation on the material. Materials having such a property are used generally as sensors and transformers. The structural properties of ZnO provides it a powerful piezoelectric characteristics.

- Powerful luminescence

  ZnO is a suitable material for phosphor applications since it has significant luminescence property in a wide spectral region [2]. ZnO having n-type conductivity is a popular material especially for field emission display applications.

There are also many advantages properties of ZnO in addition to above given properties. Moreover, studies on the doped ZnO with different type of elements showed that there can be new application areas of doped ZnO.

In the present thesis, the characteristics of defect centers in aluminum doped ZnO (AZO) nanocrystals obtained from the thermoluminescence measurements are presented. Defects are structures destroying the crystalline periodicity of the material. The missing atoms in the regular lattice positions (holes), extra atoms in the regular lattice points, oxygen substituting for zinc or zinc substituting for oxygen are some of the defect types. Defects and/or impurities bring about existence of energy states called as trapping centers in the band gap of the sample. Defects significantly affect optical and electrical properties of material such minority carrier lifetime, luminescence efficiency and diffusion mechanisms [4]. For that reason, revealing of the physical parameters of these centers takes importance for the scientist studying on the relevant material. Thermoluminescence (TL) is an experimental technique used for many years to investigate the properties of dosimetric materials and trapping centers existing in the forbidden band gap because of different type of defects in the studied sample. TL is based on filling of trapping centers subjected to radiation at certain temperature and the radiative emission of trapped charge carriers by making

appropriate transitions when the sample is heated. As a result of the analysis of the temperature dependence of emission intensity, kinetic parameters like trap depth, carrier concentration, frequency factor, capture cross section are obtained.

There has been an increasing attention on ZnO since it is used in low voltage luminescence applications. ZnO is known as phosphor emitting green light when it is irradiated with a light source having wavelength of 385 nm [5]. In the recent years, studies on the usage of ZnO in field emission display application have been increasing. The energy absorption in the ZnO takes place when electrons in valence band are excited to the conduction band. As a result of this absorption, a hole is created in the valence band. Recombination takes place via electronic defects and/or these holes [6]. Defects depending on different factor such morphology, structure, particle size, composition and crystallinity have an important role in the luminescence device technology. It is very important to get information about the emission mechanisms in ZnO material because of its usability in field emission display and other optical or optoelectronic device applications.

Previously Lima et al. [7] plotted a diagram showing energy levels in the band gap of ZnO semiconductors under the light of results of emission spectra of the sample. Figure 1.1 shows the reported diagram and transitions within the band gap. In the diagram, solid, dotted and hyphen arrows present non-radiative transitions, possible red and green emissions, respectively.

Bixia Lin et al. reported the below given diagram (Figure 1.2) prepared under the light of results of photoluminescence measurements on ZnO films and some theoretical information [8]. They attributed the observed peak at 3.18 eV to the transition between conduction and valence bands, and 2.38 eV to the transition from valence band to defect center existing due to antisite O_{Zn}.

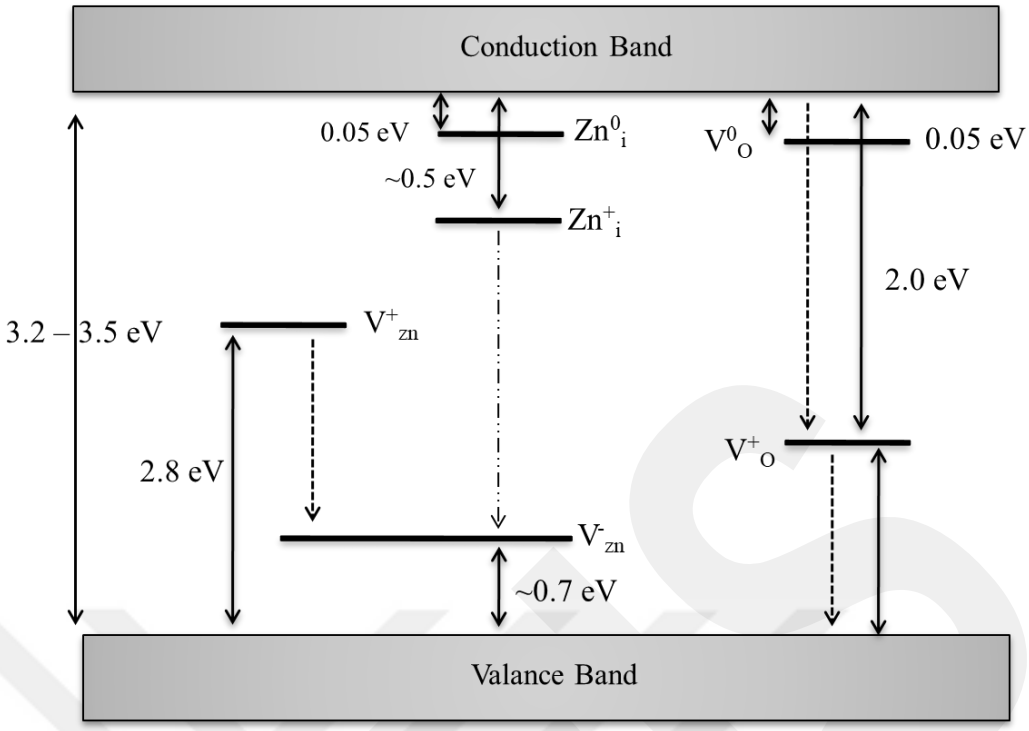

Figure 1.1 Diagram showing electronic levels and transitions in ZnO [7].

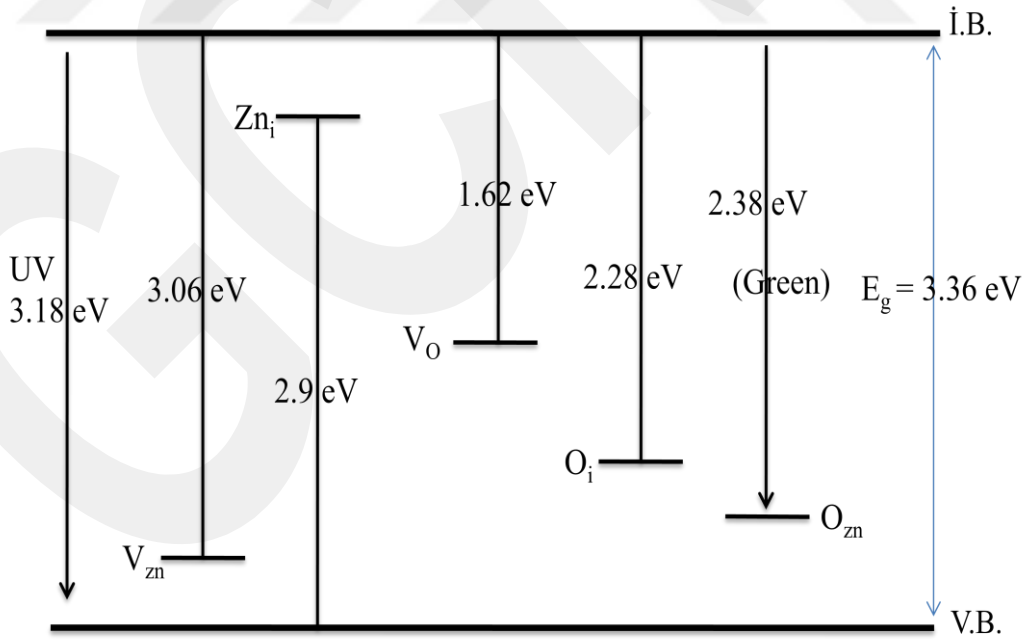

Figure 1.2 Diagram showing energies of defect centers calculated in ZnO thin films [8].

Another study was performed by Xu et al. [9] to investigate the energy levels within the forbidden band gap. Authors reported the diagram in Fig. 1.3 using the results of their theoretical calculations of full-potential linear Muffin-tin orbital (FP-LMTO) method.

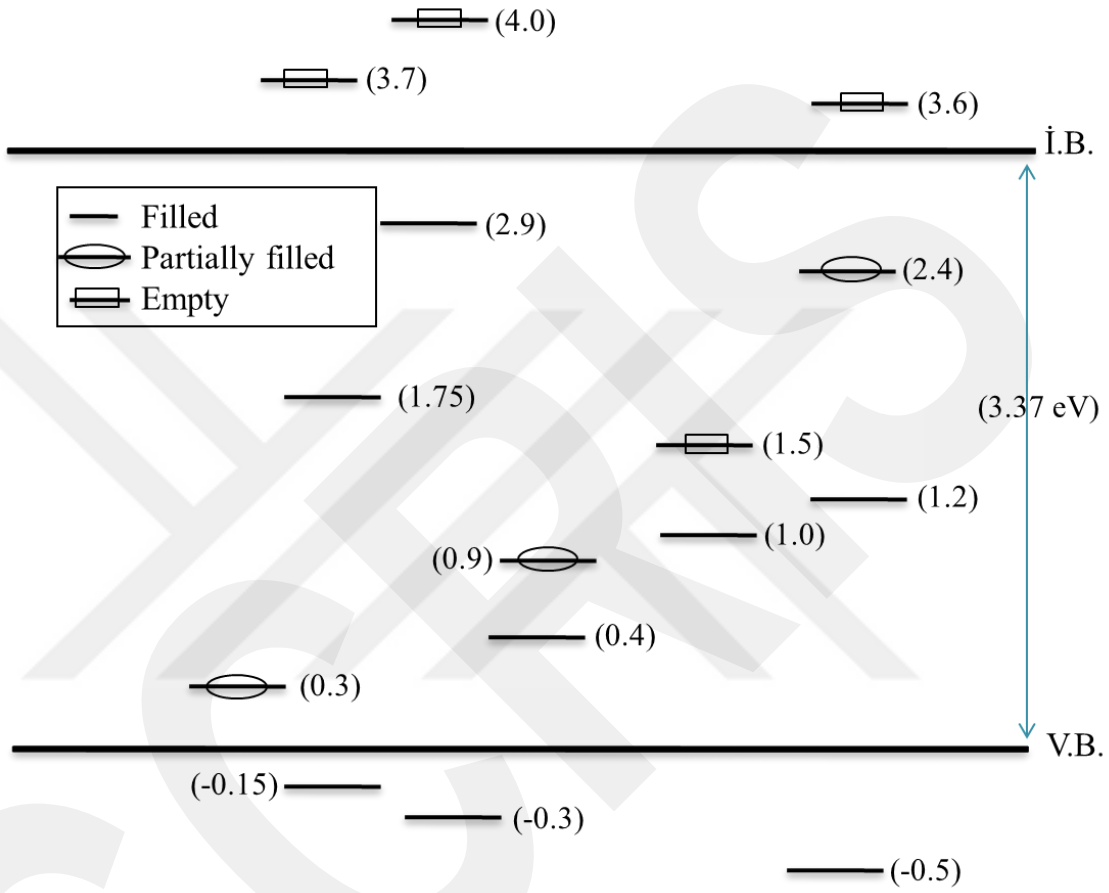

Figure 1.3 The positions of intrinsic point defect centers in ZnO calculated using FP-LMTO method [9].

Thermoluminescence (TL) is one of the experimental techniques used for years for some specific purposes. The widest usage area of TL is to investigate dosimetric materials. Another usage aim of the TL is to reveal the defect centers in semiconductors and insulators. Defects causing the existence of trapping centers within the band gap affect performance (or optical properties) of the devices. Therefore, characterization of defect centers should be done to improve the quality of the technological devices. The present thesis investigates the defect centers in

aluminum doped ZnO nanoparticles. In the literature, there are many studies on the thermoluminescence properties of ZnO structures.

Wnag et al. investigated the low temperature TL properties of the ZnO single crystals [10]. Authors attributed the observed peaks to the missing oxygen atoms and then gave information about the formation of crystal structure.

A.J. Reddy et al. performed the TL measurements on gamma irradiated ZnO nanostructures above room temperature [11]. They observed peak at ~ 343 ^{o}C and attributed this peak to defects related with oxygen. The activation energy of the defect center associated with the observed peak was found as 0.52 eV.

C. Cru-Vazquez et al. investigated the TL properties of beta irradiated ZnO nanophosphors [12]. The glow curve exhibited one wide peak around 220 ^{o}C. Authors concluded from the results of dose dependence TL glow curves that ZnO nanophosphors are promising materials to be used in dosimetry area.

U. Pal et al. reported the TL properties of Yb doped ZnO material [13]. TL experiments accomplished between 300-600 K presented the existence of two peaks around 420 and 490 K for undoped ZnO amd one peak around 480 K for 5% Yb doped ZnO sample. It is observed that peak height significantly decreases for doped sample. Analyses resulted in activation energies of 0.8 eV (420 K), 1.2 eV (490 K) and 0.8 eV (480 K). Researchers concluded that studied nanophosphors can be used in dosimetric investigations.

H.A. Borbon-Nunez et al. investigated the TL characteristics of ZnO phosphors sintered at different temperatures and for the dose range of 25-800 Gy [14]. Analyses of the glow curves showed that observed TL peak consisting in six individual peak for all samples. The peak maximum temperature, activation energy and kinetic parameters of each peak were obtained. Moreover, authors reported that sample sintered at 1173 K shows the best dosimetric characteristics.

J. Manam et al. reported the TL properties of ZnO phosphors irradiated with x-rays for different times [15]. Two overlapped peaks at 116 and 207 ^{o}C were observed as a result of experiments performed in the temperature range of 0-325 ^{o}C and radiation dose range of 200-1200 mGy. The activation energies of the trapping centers were found from the analyses as 1.01 and 0.42 eV. Moreover, the peak at 207 ^{o}C showed good sensitivity in the x-ray irradiated ZnO phosphors at room

temperature. Under the light of this result, authors reported that ZnO can be used as detector for x-rays and dosimetric material.

A.J. Reddy et al. carried out the TL measurements in the above room temperature region on the Eu doped ZnO nanoparticles [16]. One wide peak centered around 355 ^{o}C was observed in the TL glow curve obtained for samples given doses in the range of 1-10 kGy. The analyses indicated that this one wide peak consists in five individual peaks related with trapping centers having energies between 0.20 and 1.26 eV.

P.P. Pal et al. investigated the TL properties of Eu^{3+} and Tb^{3+} doped ZnO nanorods [17]. TL glow curves of Eu^{3+} and Tb^{3+} doped ZnO samples presented peaks around 365 ^{o}C and 350 ^{o}C, respectively. The activation energies of these peaks were found as 0.9 eV (Eu^{3+}:ZnO) and 0.8 eV (Tb^{3+}:ZnO) from the isothermal luminescence decay method. Moreover, the properties of dose dependency and reproducibility of the TL peaks indicated that studied samples can be used as TL dosimeter.

N.R. Panda et al. reported the TL characteristics of Ce doped ZnO nanopowders [18]. The analyses of the observed glow curve resulted in six different trapping centers in the band gap of the sample. In this paper, authors presented the peak maximum temperatures, activation energies and kinetic orders of each peak.

In the present thesis, the low temperature TL properties of aluminum doped ZnO nanoparticles is presented. In the literature, there are few studies on the below room temperature TL studies on doped and undoped ZnO samples. One of this studies was reported by Wang et al. Authors investigated TL properties in the temperature range of 25-280 K of two different ZnO samples bought by two different firms [10]. The glow curves of the samples exhibited three peaks; a powerful peak at 40 K and two weak peaks at 136 and 150 K.

Another study on the low temperature TL properties of ZnO powders was reported by D. De Muer and W.M. der Vorst [19]. The analyses showed that observed wide peak is consist in five individual peaks centered at 112, 129, 144, 156 and 172 K. The spectral measurements indicated that the peak at 172 K gives emission at 520 nm and other peaks give emission at 570 nm.

M.A. Seitz et al. investigated the TL behavior of ZnO polycrystals in the below room temperature region [20]. In the glow curve, one wide peak at 150 K and one individual peak at 182 K were observed. The analyses of glow peaks showed that there are one trap center at 0.4 eV associated with copper impurity and one zinc vacancy defect at 2.4 eV above valence band.

In this study, ZnO nanoparticles doped with aliminum will be synthesized using a chemical synthesis method(s). Structural properties of synthesized nanoparticles will be investigated using x-ray diffraction and scanning electron microscopy. Then, the main aim of the project, low temperature thermoluminescence measurements in the 10-300 K temperature range, will be carried out. The measurements will be expanded by varying appropriate experimental parameters (heating rate, excitation temperature etc.) depending on the observed TL glow curve. The kinetic parameters of the trapping centers will be found as a result of analysis of the obtained glow curves.

CHAPTER II

THEORETICAL APPROACH

2.1 Introduction

Semiconductor materials have a very effective position for the most of the today's technological applications. Therefore, characterization of these materials are very important from the point view of related applications. One of the factors affecting the performance of semiconductor devices is the existence of defects in crystal structure. These defect can be created intentionally or unintentionally. The defects present an additional energy level called as trap level (or trapping center) within the band gap. The main concern of this chapter to give information about semiconductors, their band structure and defects.

2.2 Band Structure of Semiconductors

The band structure of semiconductors gives a valuable position to them for device applications. Crystalline materials have periodically oriented atoms in three dimensions. Theoretical way of defining band structure is based on the solution of Schrödinger's wave equation. Under the effect of periodical potential, wave function (ψ) of an electron is given as

$$\psi(r) = u(r)\exp(\ ikr) \tag{2.1}$$

where k and r symbolize the wave vector and position vector, respectively. Bloch function $u(r)$ is also periodic according to relation of $u(r) = u(r + a)$. As mentioned above crystal structure has periodically positioned atoms. This results in a periodic potential felt by an electron inside this periodic structure. When the Schrödinger's

equation was solved under the light of assumptions given by Kronig Penney [21], wave vector dependency of energy is plotted as given in Fig. 2.1b [22]. In the figure 2.1a, wave vector dependency of energy for a free electron is also shown. For a free electron, there is no restrictions on energy. However, periodic structure of a crystalline material causes a forbidden region for electron at $k = n\pi/L$ where L indicates the width of potential barrier and n is integer.

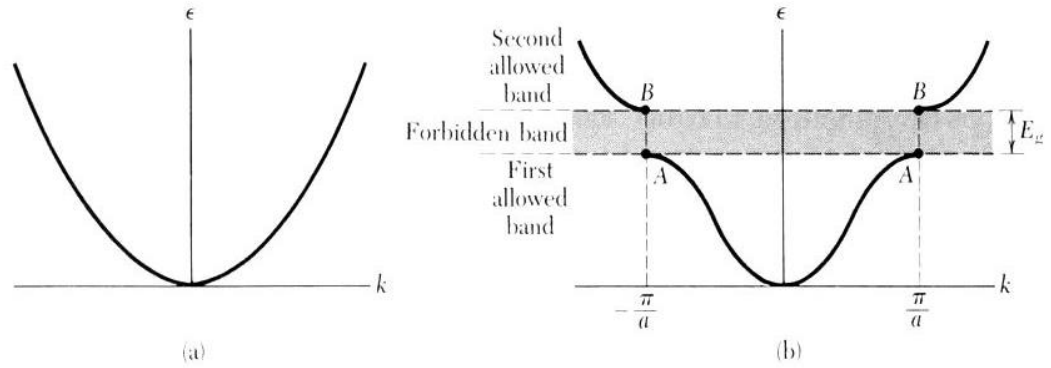

Figure 2.1 Energy-wave vector dependencies of (a) free electron (b) electron in a periodic potential [22].

According to given plot for solids, there exist energy bands to be occupied by electrons. Valence band is called as the energy band which is the highest one occupied by electrons at absolute zero temperature $T = 0$ K. The first energy band above this valence band is called as conduction band. Electrons in this band contribute to conduction of materials. At zero temperature, all electrons are found in the valence band. Electrons can excite to conduction band after getting enough energy supplied by different factor such heat, light. The energy region between the valence and conduction bands are forbidden and the energy difference is called as band gap energy. Semiconductors differ from insulators and conductors according to bigness of this energy value. In the conductors, there is very small or no band gap between the valence and conduction bands. Therefore, electrons can easily excite to conduction band. This property provides conductors a very good conductivity characteristics. In the insulators, this gap is very large and therefore electrons have

very small probability to be found in conduction band. The weak conductivity/big resistivity is a result of this fact. Semiconductors have band gap energy between those of insulators and conductors. The general gap energy range is defined as 2-3 eV for semiconductors.

2.3 Intrinsic and Extrinsic Semiconductors

One of the most important properties of semiconductors is associated with their controllable conductivity characteristics. Impurities intentionally or unintentionally doped to semiconductors affect the conductivity of semiconductors. According to presence of impurities, semiconductors are named as intrinsic and extrinsic semiconductors. Intrinsic semiconductors do not have impurities or defects within the band structure. They can also be called as perfect semiconductors which do not have free carrier. As mentioned above, electrons can excite to higher energy bands when enough energy is supplied to them. If an electron get this enough energy, it excite to conduction band by leaving a hole in valence band behind it. Since one hole is associated with one electron for intrinsic semiconductors, concentrations of electrons (n) and holes (p) is equal to each other and they are related to intrinsic carrier concentration (n_i) as

$$n.p = n_i^2 \quad . \tag{2.2}$$

Extrinsic semiconducting compounds are the materials having impurities. If impurities are added to materials intentionally, the addition process is called as doping. When a semiconducting material is doped, free charge carrier concentration increases in the crystal structure. According to type of doped element, doping is classified as *n*-type doping and *p*-type doping.

n-type doping: Silicon (Si) is one of the elements of group IV. Let's see what happens when any element from group V (pentavalent group) is added into Si-crystal. Figure 2.2a indicates the addition of phosphor (P) into Si-crystal. P has five electrons in its outermost energy level. Four of these five electrons combine with host atom. Fifth electron of doped P-atom does not involve in bonding. This electron

is weakly bonded to P-atom and therefore it can move freely within the crystal structure after getting very small energy. This type of semiconductors having excessive electrons are named as *n*-type. Weakly bonded electron to P-atom is not free, therefore it cannot be thought in conduction band. Also it cannot be thought in valence band since it can be free after having very small energy. This property which is excitability to conduction band with very small energy results in existence of an additional energy level within the forbidden band gap. This energy level is closer to conduction band as indicated in Fig. 2.3a. It can be seen as contradiction to say that there exists an energy level within the forbidden gap. Forbidden gap does not contain any energy level for perfect crystal structures. However, doped materials are no longer perfect. This energy level is called as donor level.

***p*-type doping**: The doping process of Si-crystal with en element from III group such Boron (B) creates an unbonded electron as shown in Fig. 2.2b. Since B has three valence electrons, they combine with atoms of host material. However, there remains an unbonded electron due to a missing electron. This missing electron creates a hole in the crystal. Added impurities in this materials is named as *acceptor* due to presence of holes. Doped Si-material is named as *p-type semiconductor*. Similar to free electron in n-type semiconductors, free holes create an additional energy level within the forbidden band gap. Since this hole can be excited to valence band by supplying small energy, this added energy level is closer to valence band as shown in figure 2.3b.

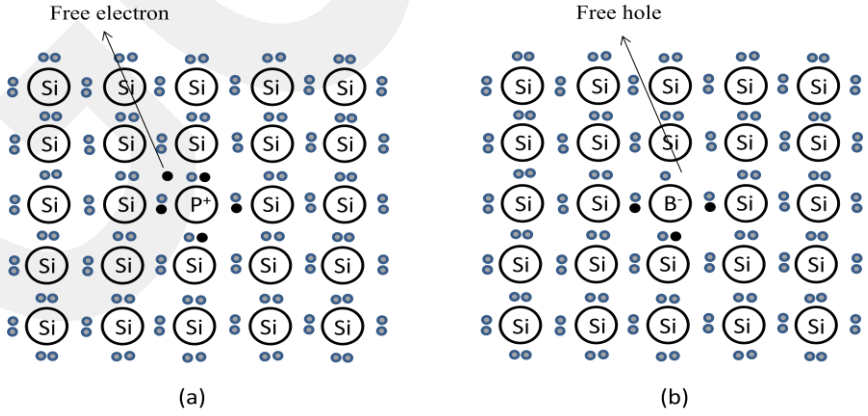

Figure 2.2. Silicon doped with (a) Phosphor (b) Boron atom.

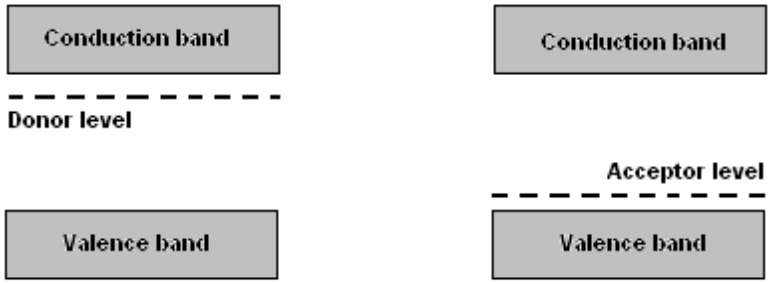

Figure 2.3. Representation of (a) donor and (b) acceptor levels.

2.4 Defects

As pointed in the previous sections, a material with crystalline structure has periodically arranged atoms. A perfect crystal has a structural property in which every atom is well-arranged. However, it is difficult or impossible to grow perfect crystals. The arrangement of the atoms can be destroyed due to some imperfections called as defects. According to dimensions, defects are classified into four groups; 0-dimensional defects (point defects), 1-dimensional defects (line defects), 2-dimensional defects (planar defects) and 3-dimensional defects (volume defects). Each defect type is defined in the following sections.

2.4.1 Point Defects

0-dimensional point defects exist at one point of a crystalline material. Figure 2.4 shows different types of point defects. The existence of open circles representing the host atom was destroyed due to presence of vacancies, substitutional large and small atoms, impurity atoms and wrong positioned host atom. As pointed in the doping story, defects also create trapping centers within the band gap.

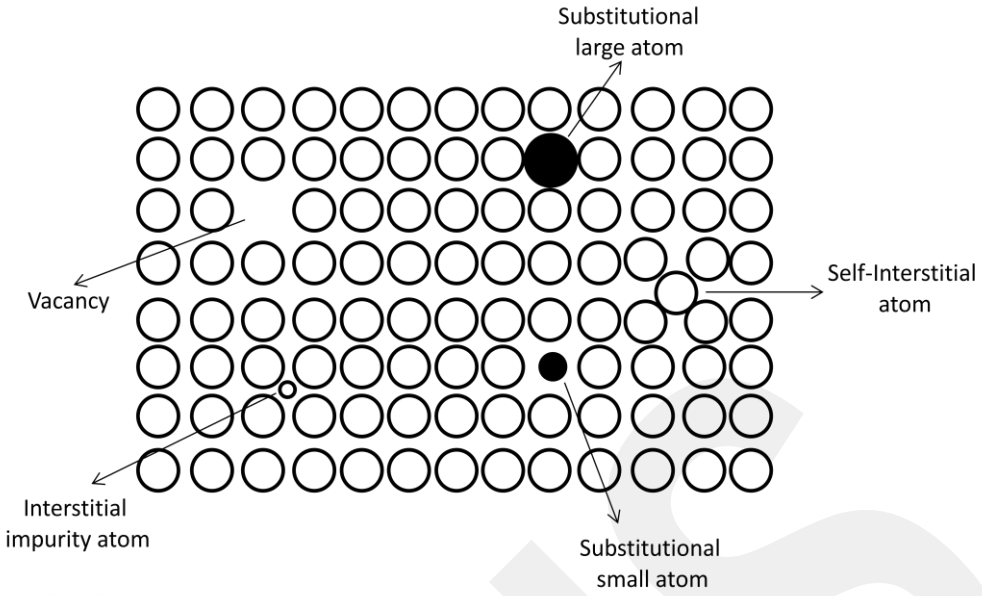

Figure 2.4. Representation of point defect types.

2.4.2 Line Defects

Instead of imperfection at one position of the crystal, there can exist disorders due to missing or wrong positioned atom groups. This imperfections are named as line defetcs or dislocations. Line defects are classified into two groups (see Fig.2.5) defined as:

i. *Edge Dislocations* is defined as the replacement (removement) of a plane to (from) crystalline structure.
ii. *Screw dislocations* is defined as shear ripple stretching from side to side

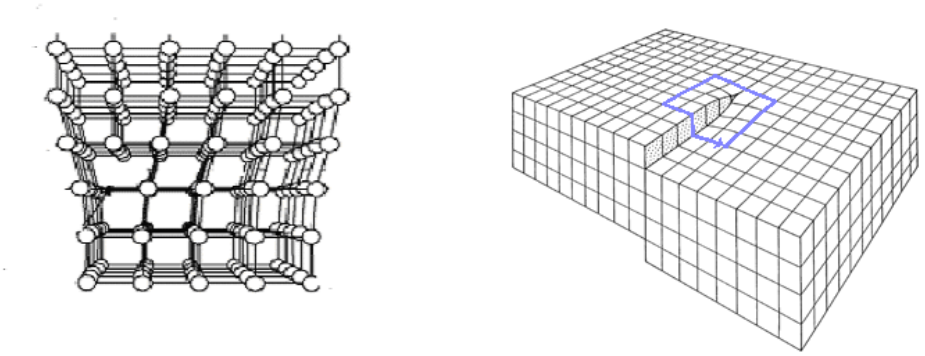

(a) (b)

Figure 2.5. (a) Edge dislocation; (b) Screw dislocation [22].

2.4.3 Planar Defects

Ideal crystalline structure can be destroyed by two dimensional planar defects. External surfaces, grain boundaries, twin boundaries and stacking faults are the types of planar defects. Stacking fault is created because of error in the sequence for a few atomic spacings. The defect type in which this error comes into existence for many atomic spacings is twin boundaries. For instance, in hexagonal structure, the crystal arrangement follows the order of MNMNMNMN. If this arrangement collapses due to addition of a new atom like O resulting in new arrangement of MNMNMNOMN, stacking fault defect is created. Besides, if the arrangement MNMNMNMN switches to MNOMNOMNO for a period of time and then returnes to initial sequence, a pair of twin boundaries is created in crystalline structure. Materials generally include many small crystallites or grains. These grains are separated by regions called as grain boundaries.

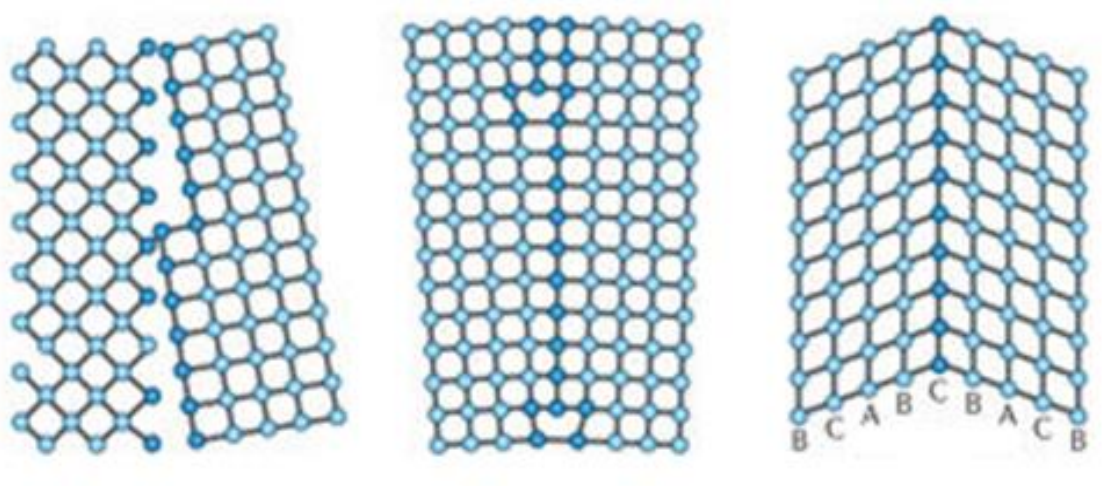

Figure 2.6. (a) High-angle grain boundary (b) Low-angle grain boundary (c) Twin boundary

2.4.4 Volume or Bulk Defects

Volume/bulk defects are three dimensional imprefections in the crystalline structure. Voids are general type of volume defects. Voids are small zones in which large amount of atoms are lost in crystalline structure. Voids are identified as clusters of vacancies. Precipitates are bulk imperfections in which impurities can cluster together and constitute small regions of different types.

2.5 X-ray Diffraction

One of the basic experimental methods used to get knowledge about the crystal structure of a material is x-ray diffraction. X-rays have wavelengths (0.01-10 nm) in the same order of magnitude with interplanar distance between atomic planes in a lattice. The x-ray diffraction method utilize from the elastic scattering of x-rays from various atoms. Figure 2.7 Indicates the deflection of x-rays (red lines) from a crystalline lattice in which planes are separated by spacing of *d*. Path variance of x-rays deflected from presented black atoms is

$$|KL| + |KM| = 2d \sin\theta \tag{2.3}$$

Deflected x-rays form constructive interference if

$$2d_{hkl}\sin\theta = n\lambda \cdot \qquad n = 0, 1, 2, 3.... \tag{2.4}$$

is satisfied. This formula is called as Bragg law [23]. In the XRD experiments, x-rays are emitted on a sample for a specific angle region. In the XRD pattern (intensity vs. angle) some intensive peaks which are results of constructive interference are observed. Analyses of peak positions are used to obtain lattice parameters of used material.

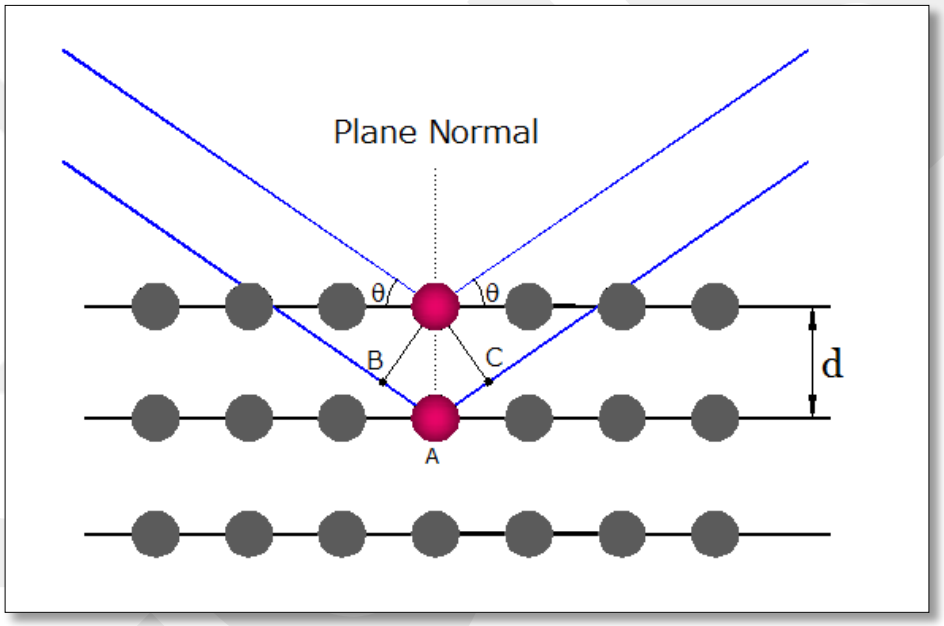

Figure 2.7 Representation of x-ray diffraction by a crystal lattice.

2.6 Thermoluminescence

Thermoluminescence is one of the main experimental techniques used to characterize the trapping centers existing within the band gap due to defects and/or impurities [24-26]. This method is used for long times on characterization of defect centers in semiconductors and insulators. Thermoluminescence name comes due to emitted luminescence from thermally heated samples. In the thermoluminescence

measurements, charge carriers making transitions between localized bands (defect/impurity centers) and delocalized bands (conduction and valence bands) takes role. Therefore, electronic transitions between these bands must be known to understand the reason of luminescence when samples are heated in thermoluminescence experiments.

2.6.1 Transitions between energy states in thermoluminescence

As mentioned in section 2.2, conduction and valence bands are separated by a energy gap in semiconductors and insulators. In perfect crystals which takes "perfect" adjective due to nonexistence of defects and impurities, there is no any energy level between these delocalized bands. However, there are evertime unintentionally existing defects and/or intentionally doped impurities in materials. These defects and impurities called as imperfections present additional energy level(s) within the band gap. Figure 2.8 shows a simple one trap (T) – one recombination (R) model on which electronic transitions are represented. The energy abbreviations E_g, E_t and E_f symbolize band gap energy, activation energy of trap center and Fermi level. Transitions between localized and delocalized bands are detailed below.

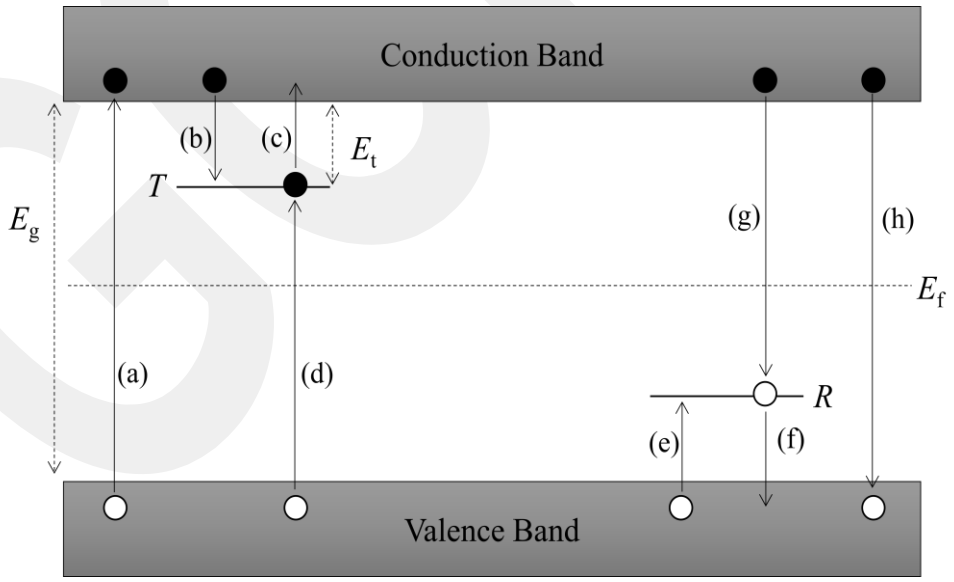

Figure 2.8. Possible electronic transitions in the TL. (a) band-to-band excitation; (b) and (e) electron and hole trapping, respectively; (c) and (f) electron and hole

releases; (d) and (g) indirect recombination; (h) direct recombination. Solid circles, open circles and arrows represent electrons, holes and transitions, respectively [24].

(I) Transition (a): When electrons in valence band gain energy greater than band gap energy, they are excited to conduction band. In semiconductors and insulators since band gap energy is relatively large, a light source is used to provide energy to electrons. The electrons excited to higher energy level leaves a empty position in valence band. This position is called as hole which is thought as positive charge. Transition (a) gets band-to-band transition name since electrons transit from valence band to conduction band.

(II) Transitions (b) and (e): There are two ways for excited electrons; recombination with holes or trapping in defect centers. Similar possibility is also valid for free holes in valence band. Transitions (b) and (e) indicates trapping of electrons and holes, respectively.

(III) Transitions (h): The second way mentioned in previous transition type is recombination of free electrons with free holes. This recombination transition is marked with "h".

(IV) Transitions (c) and (f): Trapped electrons in defect center and holes in recombination center can excite to delocalized bans when they get sufficient energy. The escape of trapped electrons and holes are indicated by transitions (c) and (f), respectively. In the TL experiments, heating provides this energy to trapped charges.

(V) Transitions (g) and (d): These transitions are indirect transitions coming existence due to recombination of opposite charge carriers. One of these carriers is in localized band whereas other one sits in delocalized band.

In the thermoluminescence measurements, material is subjected to a radiation having energy greater than band gap energy at low temperature. Electrons make band-to-band transition as a result of this radiation. When electrons return the valence band, some of them are captured by defect centers. After filling trapping centers, radiation is turned off. Trapped charge carriers have negligible probability to excite conduction band at low temperatures. In the thermoluminescence experiments, sample is heated in dark to excite trapped charges to delocalized bands. Charge carriers escaping from delocalized band make recombination with opposite charged

carriers. If this recombination is radiative, photons are emitted by sample. Intensity of luminescence which is proportional to number of emitted photns are obtained as a function of temperature. TL intensity ─ temperature plot called as TL glow curve is used to characterize the trapping centers.

2.6.2 Theoretical Equations for Thermoluminescence

Theoretical equations in thermoluminescence define the TL intensity-temperature dependency. However, there are three different kinetics in TL processes.

(I) First order of kinetics (slow retrapping): If excited electrons from trapping centers make recombination without trapped again, this kinetic takes name of first order of kinetics.

(II) Second order of kinetics (fast retrapping): As an opposite behavior of electrons mentioned in above kinetic type, excited electrons trapped more than one time in defect centers. This type of kinetics is called as second order of kinetics.

(III) General order of kinetics: This kinetic type is the mixture of above given twp types of kinetics.

TL intensity is given for each case as [24,25]

$$I_{TL} = n_0 \nu \exp\left\{ -\frac{E}{kT} - \int_{T_0}^{T} \frac{\nu}{\beta} \exp(-E/kT) dT \right\} . \tag{2.5}$$

$$I_{TL} = -\frac{dn}{dt} = \left(\frac{n_0^2}{N}\right) \nu \exp\left[-\frac{E}{kT} \right] \left[1 + \frac{n_0 \nu}{\beta N} \int_{T_0}^{T} \exp(-E/kT)\, dT \right]^{-2} \tag{2.6}$$

$$I_{TL} = n_0 \nu \exp\left(-\frac{E_t}{kT} \right) \left[1 + (b-1) \frac{\nu}{\beta} \int_{T_0}^{T} \exp(-E_t/kT) dT \right]^{-\frac{b}{b-1}} \tag{2.7}$$

Eqs. 2.5, 2.6 and 2.7 are related to slow retrapping, fast retrapping and mixed order of kinetics, respectively. In these equations, n_0 is the initial concentration of charge carriers in trap levels, ν is attempt-to-escape frequency, β is heating rate, T_0 is

beginnig temperature of heating process and *b* is the order of kinetics. *b* is between the 1 and 2 for general order of kinetics. Activation energies of the trap levels, attempt-to-escape frequency and order of kinetics are found as a result of analyses of glow curve. There are many analyses methods to calculate these parameters. Three of them used in this study; curve fitting, initial rise and peak shape methods are mentioned below.

2.6.3 Analyses methods for Thermoluminescence Curve

2.6.3.1 Curve Fitting Method

Equations relating the TL intensity to temperature were simplified previously in literature [27]. Under the light of simplified versions of equations, suitable software programs can be used to fit observed glow curves to theoretical equations. Curve fitting method depends on fitting of TL glow curve using acceptable software programs. The outcomes of fitting program give us opportunity to get activation energy, peak maximum temperature, frequency factor and order of kinetics. The software programme also helps to separate overlapped peaks when TL parameters of more than one overlapped peak were defined to software program as summation of individual peaks.

2.6.3.2 Initial Rise Method

Initial rise technique is one of the effective methods utilized for decades to find the activation energies of the defect centers [25]. Integrals in Eqs. 2.5, 2.6 and 2.7 for TL intensity for each of kinetics type are negligible in the initial ascending part of the TL curve. Therefore, these integrals is simplified in this initial part of the curve as

$$I = C \exp(-E_t / kT) \ , \qquad (2.8)$$

where *C* is constant. If the plot of ln (*I*) versus 1/*T* is drawn, a straight line with a slope of $(-E_t / k)$ is observed. The most attractive property of this method is usability for all order of kinetics.

2.6.3.3 Peak Shape Method

Peak shape method utilize from temperature values T_m, T_l and T_h to find the activation energy where T_m is the peak maximum temperature, T_l and T_h are the low and high half-intensity temperatures, respectively [25]. In the peak shape analyses three parameters, $\tau = T_m - T_l$, $\delta = T_h - T_m$ and $w = T_h - T_l$ are used. The activation energy associated with observed peak is obtained from the average of below given three energies;

$$E_\tau = \left[1.51 + 3.0(\mu_g - 0.42)\right] kT_m^2 / \tau - \left[1.58 + 4.2(\mu_g - 0.42)\right] 2kT_m \quad (2.9)$$

$$E_\delta = \left[0.976 + 7.3(\mu_g - 0.42)\right] kT_m^2 / \delta \quad (2.10)$$

$$E_w = \left[2.52 + 10.2(\mu_g - 0.42)\right] kT_m^2 / w - 2kT_m \ , \quad (2.11)$$

where $\mu_g = \delta/w$. The μ_g parameter is reported as 0.42, 0.52 and between these values for first, second and general order of kinetics, respectively [24,25].

CHAPTER III

EXPERIMENTAL DETAILS

Thermoluminescence experiments were accomplished on Al-doped ZnO (AZO) nanoparticle in the low temperature region. In addition to thermoluminescence properties, structural properties of doped nanoparticles were investigated using x-ray diffraction (XRD), energy dispersive spectroscopy (EDS) and scanning electron microscopy (SEM). Details of the applied experimental techniques and used devices are given in the present chapter.

3.1 X-ray Diffraction

AZO nanoparticles were investigated to reveal their crystal structure using X-ray diffraction experiments. Figure 3.1 shows "Rigaku miniflex" diffractometer used for experiments. It works with CuKα radiation (λ = 0.154049 nm). The measurements were done using powder form of the doped nanoparticles in the diffraction angle range of 10-90^{o}. The observed XRD pattern was analyzed using "DICVOL 04" software program.

3.2 Scanning Electron Microscopy

Information about the surface morphology nanoparticles was obtained using Nova NanoSEM 430 scanning electron microscope shown in Fig. 3.2.

Figure 3.1 Rigaku miniflex diffractometer.

Figure 3.2 Nova NanoSEM 430 scanning electron microscope

3.3 Thermoluminescence Measurements

The powder form of AZO nanoparticles was pressed to get pellets in the form of disks of diameter 10 mm and thickness of ~1 mm and these pellets were used for TL experiments. The pellets were pasted to a metallic surface using silver and then placed inside a closed cycle helium gas cryostat (Advanced Research Systems, Model CSW-202) cooling the environment of sample to low temperature of 10 K. LakeShore Model 331 temperature controller was employed to increase temperature linearly up to room temperature. Figure 3.3 indicates the diagram of the used home-made system for thermoluminescence experiments.

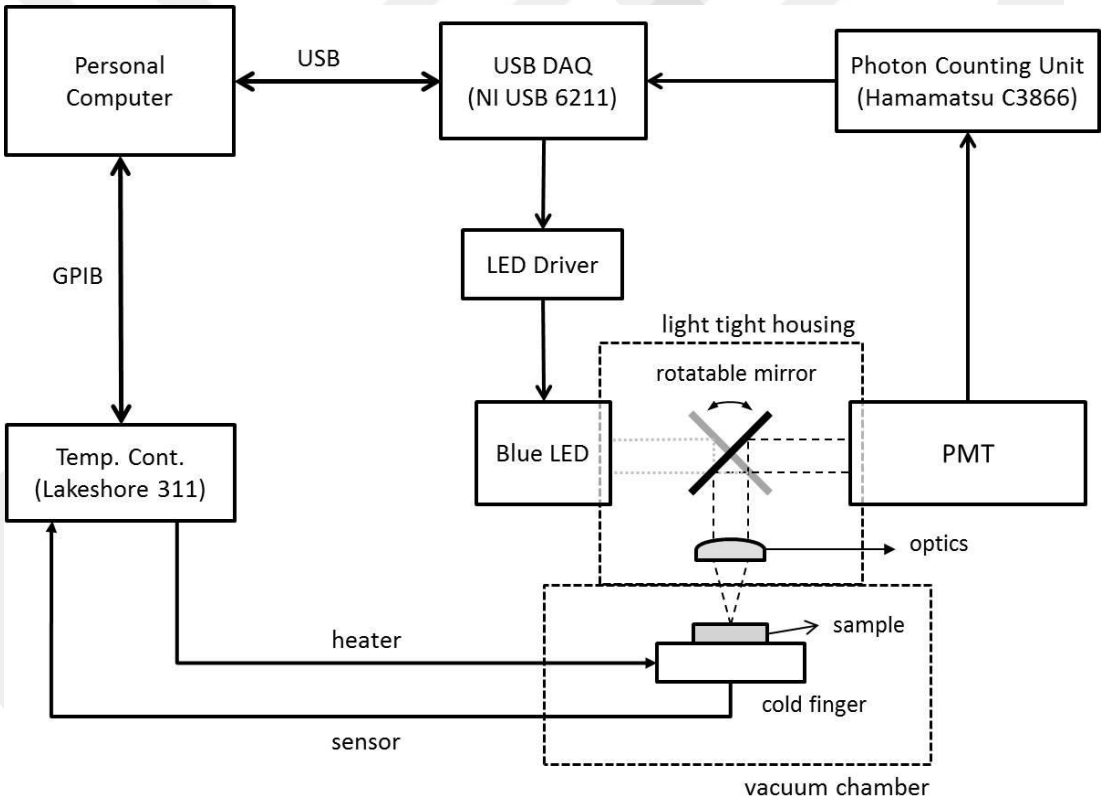

Figure 3.3 Simple diagram of low temperature thermoluminescence set-up [28].

Throughout the heating process emitted photons was collected by lenses, which focus the light to the photomultiplier (PM) tube (Hamamatsu R928, spectral response: 185-900 nm). PM tube pulses due to emitted luminescence were converted into TTL pulses (0-5 V) by a fast amplifier/discriminator (Hamamatsu Photon Counting Unit C3866). Counter of a data acquisition module (National Instruments, NI 6211) counted the TTL pulses. The whole system was controlled by LabView (National Instruments). The general procedure of applied TL experiments on AZO nanoparticles can be summarized as follows: AZO pellets were illuminated by ultraviolet LED at 10 K for 120 s. The sample was kept in dark nearly 300 s and then heated at constant rate of β = 0.1 K/s up to room temperature. For the heating rate dependent TL measurements, β was changed between 0.1 and 0.7 K/s.

CHAPTER IV

RESULTS AND DISCUSSION

4.1 Results of X-ray Diffraction Experiments

X-ray diffraction experiments were carried out on Al-doped ZnO (AZO) nanoparticles in the 2θ range of 10-70º. XRD patterns obtained from the powder forms of the doped and undoped nanoparticles are indicated in Fig. 4.1. As can be seen from the figure, observed peaks in each pattern are at the same angle position. Nonexistence of impurity peaks due to doped aliminium is a powerful indication of good purity of nanoparticle formation. The peaks observed in the pattern is well matched with standard data of JCPDS 89-0510 which reports the crystal structure as hexagonal with lattice parameters of a = 0.3249 nm and c = 0.5205 nm.

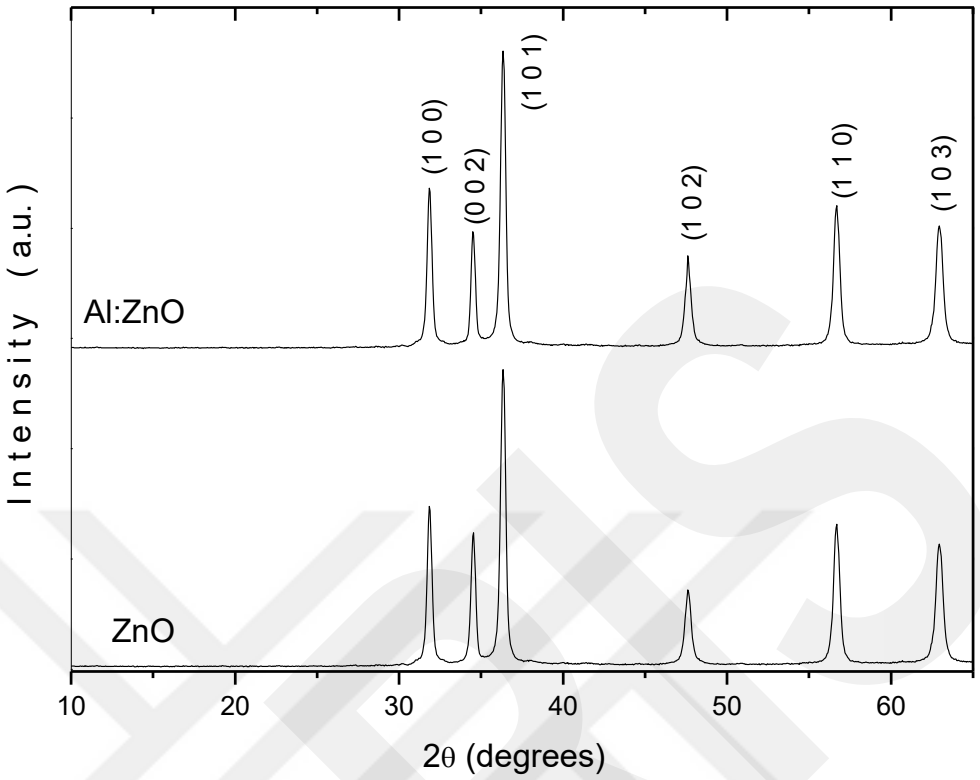

Figure 4.1 XRD diffraction patterns of doped and undoped ZnO nanoparticles

4.2 Scanning Electron Microscopy Images

Scanning electron microscopy (SEM) images were recorded to obtain information about the surface morphology of AZO nanoparticles. Figure 4.2 shows SEM images of AZO nanoparticles used as powder form in measurements for two different resolutions. The dimensions of some particles are presented on the figure. The general dimension range for nanoparticles were between 80-140 nm.

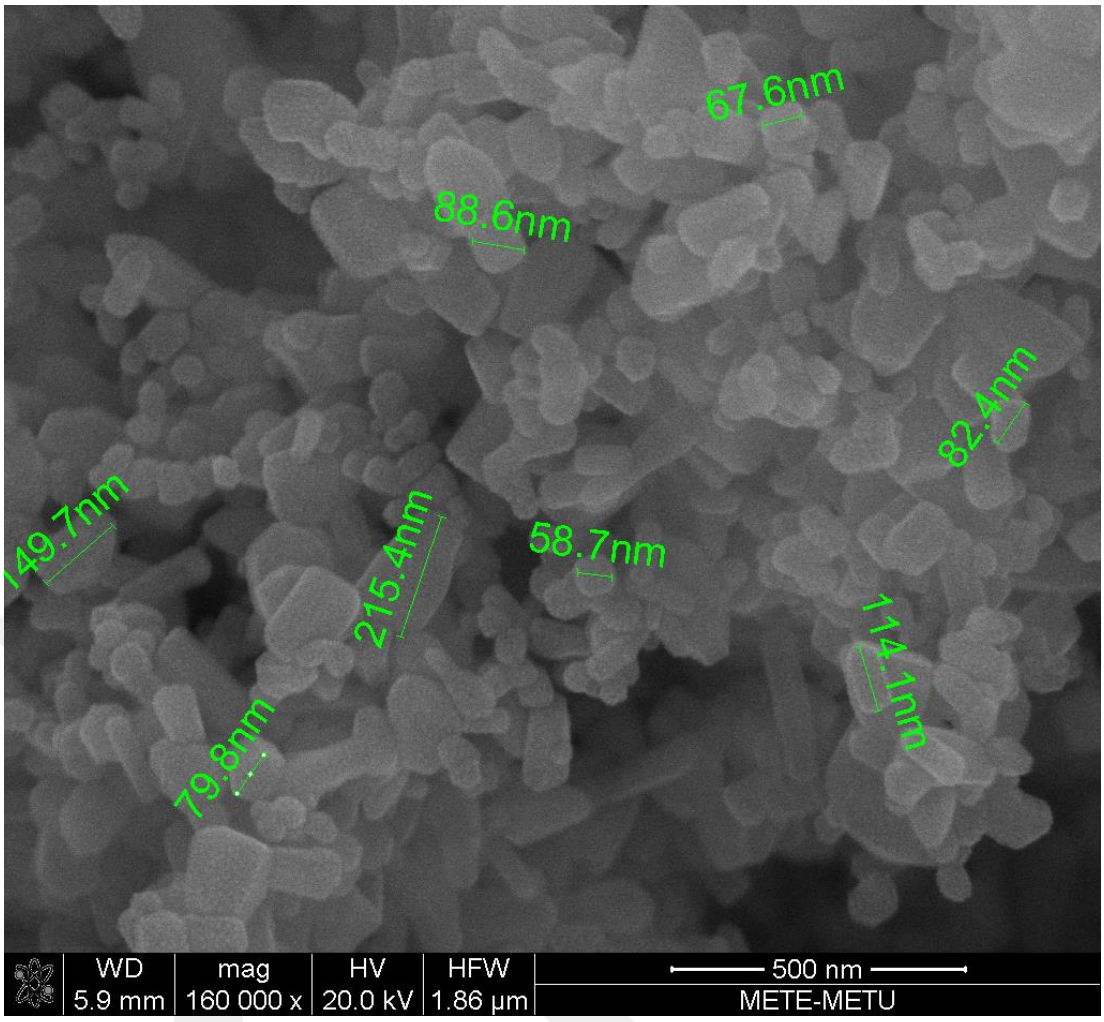

Figure 4.2 SEM images of AZO nanoparticles.

4.3 Results of Thermoluminescence Experiments

Figure 4.3 shows the experimentally observed TL glow curve (circles) obtained at constant heating rate of 0.1 K/s. TL curve exhibits one intensitive peak around 123 K and two overlapped peaks; one of them is nearly around 85 K and other one positioned around 150 K. In the literature there are many methods to find the trapping parameters such activation energy and frequency factor of the trap centers associated with peaks consisting in whole TL curve. In the present study, TL

curves were analyzed using curve fitting, initial rise, peak shape and different heating rate methods.

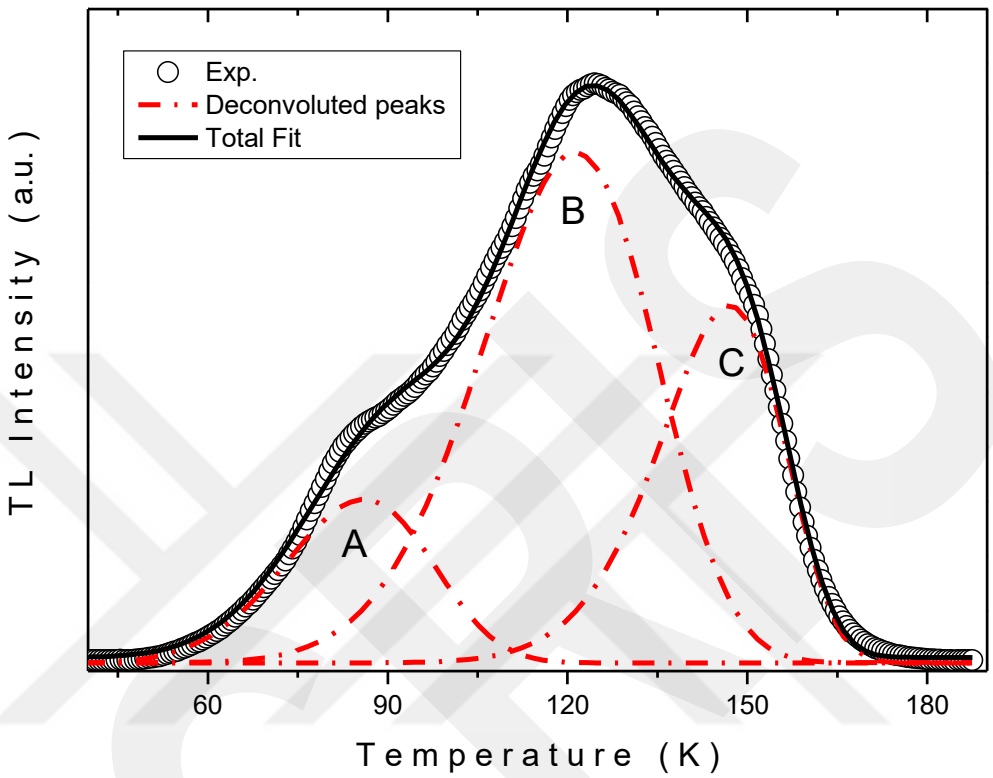

Figure 4.3. TL glow curve of AZO nanoparticles for constant heating rate of 0.1 K/s. Circles are experimental data, solid line presents total fit and dash-dotted curves are deconvoluted peaks.

Curve fitting is based on fitting of experimentally observed TL glow curve under the light of theoretical equations relating the TL intensity to temperature [27]. TL equations differ for first, second and general order of kinetics. We have tried to fit TL curve using equations related for each of order of kinetics. The most successful and acceptable fitting result were obtained for general order of kinetics. Solid curve in Fig. 4.3 is the fitted curve and dash-dotted curves are deconvoluted peaks which are associated with three different trapping centers. Curve fitting analyses resulted in

activation energies of 44, 76 and 165 meV with peak maximum temperatures of 86.2, 121.5 and 147.1 K, respectively. Peaks are labelled as A, B and C on the TL curve to simplify the expression. Table 4.1 presents the result of curve fitting method.

As a second analyses method, initial rise method was applied on revealed TL peaks. As stated in sec. 2.4.3.2, the integrals in the theoretical equations are negligible. When the integrals given in Eqs. 2.5, 2.6 and 2.7 are taken as zero, it is seen that logarithm of TL intensity is proportional to exp ($-E_t/kT$). This proportionality is used to find the activation energy of the trapping centers from the plot of $\ln(I_{TL})$ vs. $1/T$. The slope of the line existing in the relevant plot gives ($-E_t/k$) and this slope helps us to calculate the of activation energy. Figure 4.4 shows the mentioned plots for each revealed TL peaks. The activation energies of the trapping centers were found as E_{tA} = 44 meV, E_{tB} = 74 meV and E_{tC} = 162 meV (see Table 4.1). These results are in good agreement with those obtained from curve fitting analyses technique.

Table 4.1. Activation energies (E_t), peak maximum temperatures (T_m), and peak shape method parameter (μ_g)

Peak	T_m (K)	E_t (meV)			μ_g
		Curve fitting method	Initial rise method	Peak shape method	
A	86.2	44	44	49	0.46
B	121.5	76	74	85	0.45
C	147.1	165	162	170	0.43

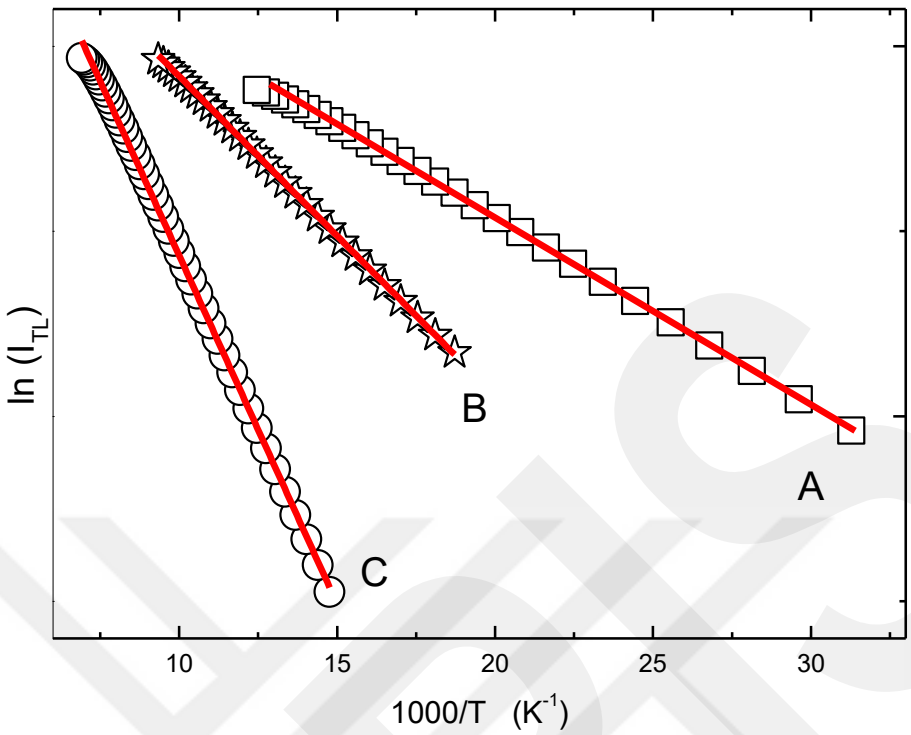

Figure 4.4. Initial rise method plots for each revealed TL peaks.

Peak shape method was also applied to get activation energies and kinetic types [25]. The average values of activation energies E_ζ , E_δ and E_w given in section 2.4.3.3 were calculated as E_{tA} = 49 meV, E_{tB} = 85 meV and E_{tB} = 170 meV (Table 4.1). The μ_g parameter for these peaks were calculated and found between 0.42 and 0.52 which indicates the presence of general order of kinetics. All found activation energy values of peaks by curve fitting, initial rise and peak shape methods are in good agreement with each other.

Heating rate dependencies of TL curves were investigated for the rates ranging from 0.1 K/s to 0.7 K/s. The observed glow curves are indicated in Fig. 4.5. According to theoretical equations, heating rate is directly proportional to peak maximum temperature. As can be seen from the figure, this theoretical expectation is satisfied for observed TL curves.

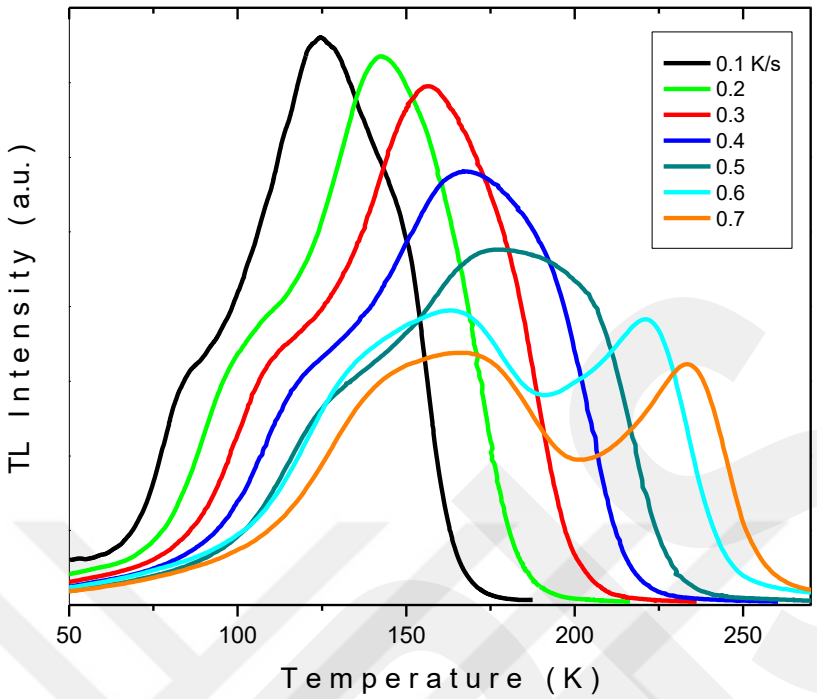

Figure 4.5. TL glow curves obtained at different heating rates.

Although shift of peak maximum temperature to higher values are satisfied for the rates between 0.1 to 0.5 K/s, TL curves obtained at 0.6 and 0.7 K/s show a different behavior with increase of heating rate. If peak maximum position of peak A was carefully looked, it is seen that theoretical expectations are satisfied. This is also valid for peak C which is not clearly seen due to overlapping situation for rates between 0.1 and 0.5 K/s. However, peak maximum values of this peak is easily read for rates of 0.6 and 0.7 K/s. This result is due to decrease of peak maximum temperature of peak B after β = 0.5 K/s. Since peak maximum temperature decreases when TL curve is observed for 0.6 K/s, peaks B and C seems to be separated as seen in the figure. Figure 4.6 shows the heating rate dependent peak maximum temperature values.

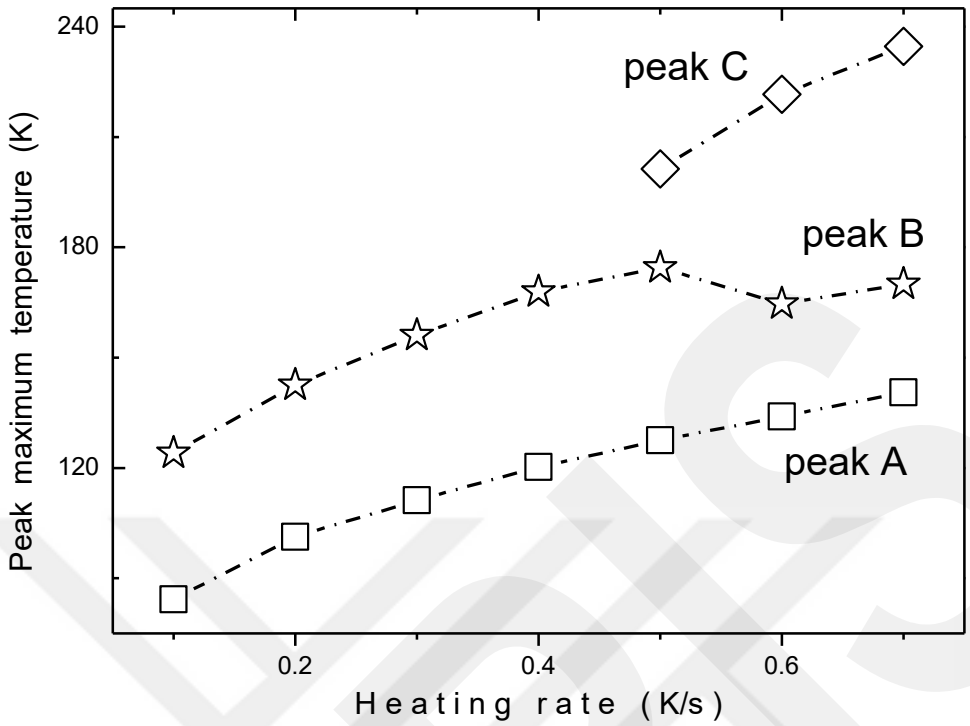

Figure 4.6. Heating rate dependency of peak maximum temperatures.

Heating rate dependent TL curves are also used to find the thermal activation energies of the trapping centers. Peak maximum temperature ─ heating rate dependency is expressed by the relation [18]

$$\beta = (sk / E_t)T_m^2 \exp(-E_t / kT_m) \tag{4.1}$$

In the Eq. 4.1, right part contains two T_m dependent mathematical expression. However, exponential part is dominant peak maximum temperature dependent factor. For that reason, β is proportional to exp ($-E_t/kT$) according to this equation. ln(β) - 1/T graph results in linear behavior with a slope of ($-E_t/kT$). Before applying this method for our TL curves, we have made corrections on peak maximum temperature according to Ref. [29]. One of the problems for heating rate dependent experimental data is the temperature lag effect. This problem exist due to differences between the

real temperature of the sample and temperature value read by temperature sensor. In the low temperature region, this problem affects the data much more than the data obtained in the high temperature region. In the literature, there are some studies concerning this problem. One of this studies was reported by Kitis and Tuyn in Ref. [29]. Researchers introduced a technique to minimize this temperature gradient. Experimentally obtained T_m values were corrected using the relation

$$T_{mj} = T_{mi} - c \ln\left(\frac{\beta_i}{\beta_j}\right) \tag{4.2}$$

where T_{mi} and T_{mj} symbolize the peak maximum temperatures of TL curves observed for rates of β_i and β_j, respectively and c is a constant. We have performed heating rate analyses method and temperature lag effect for peaks A and B since peak maximum temperature value of peak C cannot be read easily for the rates between 0.1 and 0.5 K/s due to overlapping problem.

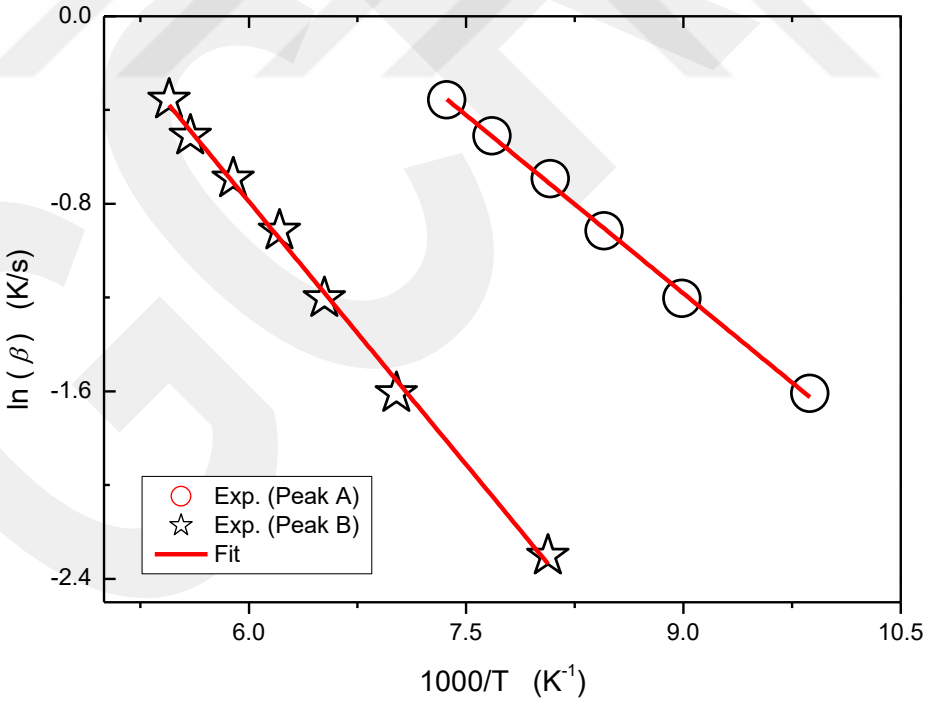

Figure 4.7. The plot of ln(β) vs. 1000/T_m.

Under the light of Eq. 4.2, c values were found for peaks A and B as c_A = 24.5 K and c_B = 26.7 K. After making corrections for peak maximum temperature values, ln(β) - 1/T plots were drawn as shown in Fig. 4.7. Both plot present linear behavior and linear fitting of these plots resulted in activation energies of E_{tA} = 44 meV and E_{tB} = 65 meV. When these values were compared above given results obtained from curve fitting, initial rise and peak shape methods, a very good agreement can be seen.

CHAPTER V

CONCLUSION

Structural and thermoluminescence properties of Al-doped ZnO nanoparticles were reported in the present thesis. X-ray diffraction, energy dispersive spectroscopy and scanning electron microscopy measurements were applied for structural characterization whereas thermoluminescence experiments were carried out on a home-made experimental system around a closed cycle helium cryostat. Thermoluminescence properties of doped nanoparticles were studied in the below room temperature region.

XRD peaks of doped and undoped ZnO nanoparticles were observed at the same angle position. Nonexistence of any peaks associated with doped element was attributed to powerful indication of good purity of nanoparticle formation. The analyses of the XRD diffraction pattern resulted with a well matched lattice Miller indices and lattice parameters of doped sample with standard data which reports the crystal structure as hexagonal. Scanning electron microscopy images was recorded to get information about the surface morphology of AZO nanoparticles. The dimensions of nanoparticles were observed around 100 nm.

TL glow curve exhibited one intensive peak around 123 K and two overlapped peaks around 85 K and 150 K. TL curves were analyzed using curve fitting, initial rise, peak shape and different heating rate methods. The most successful and acceptable fitting result were obtained for general order of kinetics under the light of three deconvoluted peaks which are associated with three different trapping centers at 44, 76 and 165 meV with peak maximum temperatures of 86.2, 121.5 and 147.1 K, respectively. The activation energies of the trapping centers were found as E_{tA} = 44 meV, E_{tB} = 74 meV and E_{tC} = 162 meV from the initial rise

method. Peak shape method was also used to get activation energies and kinetic types. The activation energies were calculated as E_{tA} = 49 meV, E_{tB} = 85 meV and E_{tB} = 170 meV. The μ_g parameter for observed peaks were found between 0.42 and 0.52 indicating the presence of general order of kinetics. Heating rate dependencies of TL curves were investigated for the rates ranging from 0.1 K/s to 0.7 K/s. The increase of peak maximum temperature to higher values and decrease of TL intensity with increasing heating rate were observed as a result of experimental observations. Activation energies of trapping centers were found using heating rate dependency of peak maximum temperature. We applied heating rate analyses technique and temperature lag effect for peaks A and B since peak maximum temperature value of peak C cannot be read easily for the rates between 0.1 and 0.5 K/s due to overlapping problem. ln(β)-1/T plots were drawn and and linear fitting of these plots resulted in activation energies of E_{tA} = 44 meV and E_{tB} = 65 meV.

REFERENCES

[1] A. Mang, K. Reimann, St. Rübenacke, *Band gaps, crystal-field splitting, spin-orbit coupling, and exciton binding energies in ZnO under hydrostatic pressure*, Solid State Communications 94 (1995) 251-254.

[2] N.H. Nickel, E. Terukov, *Zinc Oxide-A material for micro and optoelectronic applications*. Netherlands: Springer, 2005.

[3] D. M. Bagnall, Y. F. Chen, Z. Zhu, T. Yao, S. Koyama, M. Y. Shen, T. Goto, *Optically pumped lasing of ZnO at room temperature*, Applied Physics Letters 70 (1997) 2230-2232.

[4] M. Lannoo, J. Bourgoin, *Point Defects in Semiconductors II: Experimental Aspects*. Berlin: Springer, 1981.

[5] D. Kouyate, J. C. Ronfardharet, P. Valat, J. Kossanyi, U. Mammel, D. Oelkrug, *Quenching of zinc-oxide photoluminescence by d-transition and f-transition metal-ions*, Journal of Luminescence 46 (1990) 329-337.

[6] G. Blasse, B. C. Grabmaier, *Luminescent Materials*. Berlin: Springer, 1994.

[7] S. A. M. Lima, F. A. Sigoli, M. Jafelicci, M. R. Davolos, *Luminescent properties and lattice defects correlation on zinc oxide*, International Journal of Inorganic Materials 3 (2001) 749-754.

[8] B. Lin, Z. Fu, Y. Jia, *Green luminescent center in undoped zinc oxide films deposited on silicon substrates*, Applied Physics Letters, 79 (2001) 943-945.

[9] P. S. Xu, Y. M. Sun, C. S. Shi, F. Q. Xu, H. B. Pan, *The electronic structure and spectral properties of ZnO and its defects*, Nuclear Instruments and Methods in Physics Research B 199 (2003) 286-290.

[10] Y. Wang, B. Yang, N. Can, P. D. Townsend, *Correlations between low temperature thermoluminescence and oxygen vacancies in ZnO crystals*, Journal of Applied Physics, 109 (2011) 053508.

[11] A. J. Reddy, M. K. Kokila, H. Nagabhushana, J. L. Rao, C. Shivakumara, B. M. Nagabhushana, R. P. S. Chakradhar, *EPR, thermo and photoluminescence properties of ZnO nanopowders*, Spectrochimica Acta Part A: Molecular and Biomolecular Spectroscopy, 81 (2011) 59-63.

[12] C. Cruz-Vazquez, R. Bernal, S. E. Burruel-Ibarra, H. Grijalva-Monteverde, M. Barboza-Flores, *Thermoluminescence properties of new ZnO nanophosphors exposed to beta irradiation*, Optical Materials, 27 (2005) 1235-1239.

[13] U. Pal, R. Melendrez, V. Chernov, M. Barboza-Flores, *Thermoluminescence properties of ZnO and ZnO:Yb nanophosphors*, Applied Physics Letters, 89 (2006) 183118.

[14] H. A. Borbon-Nunez, C. Cruz-Vazquez, R. Bernal, G. Kitis, C. Furetta, V. M. Castano, *Thermoluminescence properties of sintered ZnO*, Optical Materials, 37 (2014) 398-403.

[15] J. Manam, S. Das, A. Isaac, *Preparation, characterization and thermally stimulated luminescence of ZnO nanophosphors*, Indian Journal of Physics, 83 (2009) 1407-1419.

[16] A. J. Reddy, M. K. Kokila, H. Nagabhushana, C. Shivakumara, R. P. S. Chakradhar, B. M. Nagabhushana, R. H. Krishna, *Luminescence studies and EPR*

investigation of solution combustion derived Eu doped ZnO, Spectrochimica Acta Part A: Molecular and Biomolecular Spectroscopy, 132 (2014) 305-312.

[17] P. P. Pal, J. Manam, *Enhanced luminescence of ZnO:RE^{3+} (RE = Eu, Tb) nanorods by Li^{+} doping and calculations of kinetic parameters*, Journal of Luminescence, 145 (2014) 340-350.

[18] N. R: Panda, B. S. Acharya, T. B. Singh, R. K. Gartia, *Thermoluminescence and decay studies on cerium doped ZnO nanopowders*, Materials Letters, 95 (2013) 205-208.

[19] D. DeMuer, W. Maenhout, *Thermoluminescence of ZnO powder*, Physica, 39 (1968) 123-&.

[20] M. A. Seitz, W. F. Pinter, W. M. Hirthe, *Thermoluminescence of ZnO*, Materials Research Bulletin, 6 (1971) 275-&.

[21] R. L. Kronig, W. G. Penney, *Quantum Mechanics of Electrons in Crystal Lattices*. Proc. Roy. Soc. (London). 130 (1930) 499-513.

[22] C. Kittel, *Introduction to Solid State Physics*, Wiley, New York, 1971.

[23] W. L. Bragg, *The reflection of x-rays by crystals*, Proceedings of the Royal Society of London Series A. 17 (1913) 43-53.

[24] S. W. S. McKeever, *Thermoluminescence of solids*, Cambridge Uni. Press, Cambridge, 1985.

[25] R. Chen, Y. Kirsh, *Analysis of Thermally Stimulated Processes*, Pergamon Press, Oxford, 1981.

[26] A. J. J. Bos, *Theory of Thermoluminescence*, Radiat. Meas. 41 (2007) S45-S56.

[27] N. S. Yuksek, N. M. Gasanly, H. Ozkan, *Thermally stimulated current analysis of shallow levels in $TlGaS_2$ layered single crystals*. Semicond. Sci. Tech. 18 (2003) 834-838.

[28] M. Isik, E. Bulur, N. M. Gasanly, *Low temperature thermoluminescence in $TlGaS_2$ layered single crystals*. J. Lumin. 135 (2013) 60-65.

[29] G. Kitis, J. W. N. Tuyn, *A simple method to correct for the temperature lag in TL glow-curve measurements,* J. Phys. D: Appl. Phys. 31 (1998) 2065-2073.